Proceedings of the Thirty-fifth (2025) International Ocean and Polar Engineering Conference **www.isope.org**
Seoul/Goyang, Korea, June 1-6, 2025

ISBN 978-1-880653-74-6; ISSN 1098-6189

An Assessment of the Effects of Wind Turbulence on the Mooring Tensions of a Deep-Water Floating Wind Turbine

Jordi Mas-Soler, Pedro C. de Mello*, Renato M. Monaro*, Alexandre N. Simos*,*
*Paulo de T. Esperança**, Daniel F. de Carvalho e Silva****
(*) University of São Paulo, São Paulo, Brazil
(**) LabOceano, UFRJ, Rio de Janeiro, Brazil
(***) Petroleo Brasileiro SA – Petrobras, Rio de Janeiro, Brazil

ABSTRACT

Assessing the wind turbulence effects on the dynamics of Floating Offshore Wind Turbines (FOWTs) is necessary to ensure the reliability and robustness of their mooring systems. This assessment can be conducted through time-domain simulations and/or model scale tests. Nonetheless, the former are computationally intensive, while the latter are costly and require specialized facilities and equipment. Therefore, it is important to understand and have an early estimation of the impacts wind turbulence might have on the FOWT mooring dynamics. The present work aims to contribute to this understanding by investigating the issue in the scenario of a FOWT designed to operate in deep waters, using for this both model scale tests and numerical simulations. The experimental campaign was conducted in the LabOceano wave basin, using a 1:45 scale model of a semisubmersible floater, supporting a 15 MW Reference Wind Turbine (RWT), with a mooring system experimental configuration consisting of four lines. The model was tested in several design load conditions representative of Brazilian deep-water fields. The hybrid model tests emulated real-time aerodynamic loads using a set of controlled fans mounted on top of the model's tower. The experimental data was used to validate the numerical setup in OpenFAST. The validated OpenFAST setup was then adopted to simulate selected set of environmental conditions, with and without wind turbulence, enabling the quantification of its effects on the mooring tensions. Results indicate that wind turbulence predominantly affected mooring loads, with limited impact on the design tensions.

KEY WORDS: Semisubmersible FOWT; mooring dynamics; turbulence, MPM, design tensions, time-domain simulations, experimental tests, OpenFAST.

INTRODUCTION

Floating Offshore Wind Turbines (FOWTs) have become one of the most promising technologies for harnessing wind energy in the coming decades. The interest in this technology arises from the availability and reliability of offshore wind resources, the potential to increase turbine size and rated power without substantial additional investments in floater systems and mooring lines, and the availability of suitable deployment spaces. This trend is supported by recent demonstration projects installed in various locations (e.g. EQUINOR, 2022; EQUINOR, 2023; and Provence Grand Large, 2024) and collaborative efforts by several research groups to advance the technology, in particular the Offshore Code Comparison, see, for example, (IEA Wind TCP, 2022).

The development of these platforms, particularly in the early stages of a project, relies on reduced-order models, commonly in the frequency domain, to enable expedite assessments of FOWT dynamics (e.g., Hall, 2024; Mas-Soler et. al, 2024; and Hall et. al., 2022). These models are often employed in optimization frameworks that aid the selection of the floater and mooring lines during the early stages of a project, see, for example, (Karimi et. al., 2017 and Mas-Soler et. al., 2022). However, the design process for FOWTs requires extensive assessment to characterize dynamic responses resulting from hydrodynamic and aerodynamic loadings. This includes time-domain simulations and experimental testing of various Design Load Conditions (DLCs), as outlined in Classification Societies' guidelines (e.g., DNV GL AS, 2016). These DLCs define turbulence models based on turbine class for different environmental conditions and operational scenarios, suggesting a key role of the wind model in the design of the FOWT and its stationkeeping system.

Regarding the effects of wind and wind turbine operational conditions on mooring system dynamics, Lauria et. al. (2024) analyzed mooring line behavior using data from a SPAR type FOWT developed in Phase IV of the OC3-Hywind project. The analysis was conducted through numerical time-domain simulations, which were validated using experimental data from a 1:40 model scale testing campaign. The results highlight the influence of the operating wind turbine on damping contributions related to wave-induced motions and mooring line tensions, particularly in terms of increasing the operating tension range.

Similarly, Piscopo and Scamardella (2023) investigated the impact of turbulence models on mooring system selection for semisubmersible and SPAR type FOWTs, considering Ultimate (ULS), Accidental (ALS), and Fatigue (FLS) Limit State Design conditions. The study used numerical simulations for water depths ranging from 200 to 400 meters, based on

the DeepCWind platform equipped with the 5 MW NREL wind turbine. The findings indicated that turbulence models influence the mooring system design, particularly in meeting the FLS strength check criteria. The authors noted that underestimating turbulence may lead to overestimating the fatigue life of the mooring system, potentially affecting predicted maintenance costs and the operational reliability of the wind turbine.

These studies highlight the importance of accounting for turbulence effects in time-domain simulations and the evaluation of mooring line behavior under various loading conditions. However, it is unclear what is the impact of the turbulence in terms of the design tensions, which can be computed using quasi-static models and used as a criterium for selecting mooring arrangements during the first stages of a FOWT design. In this context, the present paper aims to investigate the effect of turbulence on mooring line design tensions through both experimental data and numerical simulations. The analysis is based on a semisubmersible FOWT, as described in Simos et al. (2023), designed to support the IEA-15MW RWT (Gaertner et al., 2020), with its features summarized in Table 1, and deployed at a water depth of 2000m. More specifically, this study addresses the impact of turbulence on the design tensions, with numerical simulations conducted in OpenFAST and validated against experimental data from a 1:45 scale model testing campaign. Mooring line dynamics from the time-domain simulations are presented and compared to simulations of identical DLCs under steady wind conditions. So far, the scope of the investigation has been limited to a selected set of DLCs with the wind turbine operating, defined according to DNV's guidelines (DNV GL AS, 2016).

Table 1. IEA-15MW RWT main features.

Parameter	Value	Units	Parameter	Value	Units
Cut-in wind speed	3	[m/s]	Rotor diameter	240	[m]
Cut-out wind speed	25	[m/s]	Hub diameter	3	[m]
Rated wind speed	10.59	[m/s]	Hub height	150	[m]
Rated Power	15	[MW]	RNA mass	1045	[t]
Rotor Speeds	5-7.56	[rpm]	Tower mass	1263	[t]
Blades #	3	[-]	--	--	--

MODEL SET-UP

The experimental campaign was conducted at the Ocean Laboratory at COPPE/UFRJ, which has dimensions of 40m in length, 30m in width, and a maximum depth of 15m. The tests were performed using a 1:45 scale model of a semisubmersible FOWT platform, with its main features resulting from the parametric optimization procedure described in (Mas-Soler et. al., 2022). The hull concept, optimized to support the IEA-15MW RWT in an installation site located in the Brazilian pre-salt region at 2000m water depth, is illustrated in Figure 1, with its main characteristics summarized in Table 2. Additionally, Figure 2 presents the RAOs for Surge, Heave, and Pitch motions across six different headings, providing insight into the platform's dynamic response for different wave directions.

The tests employed a Software-in-the-Loop (SiL) system developed by USP to emulate the servo-aerodynamic loads. Details of the SiL architecture used during the experimental campaign are provided in (Carmo et. al., 2024) and (C. de Mello et. al., 2024). The maximum thrust generated by the SiL system was used to define the 1:45 scale of the model.

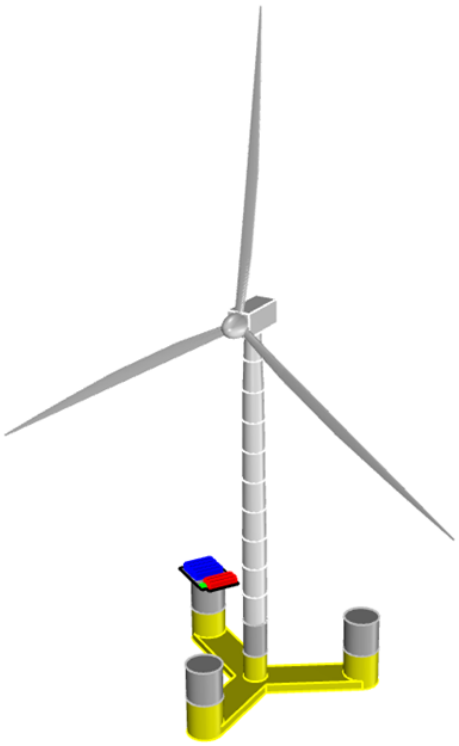

Figure 1. Schematic view of the semisubmersible FOWT concept

Table 2. Main properties of the FOWT

Parameter	Full Scale	Model Scale
Mass [ton]	15510.0	165.1 [kg]
Central col. diameter [m]	10.0	0.22
Outer col. diameter [m]	15.0	0.33
Port and Starboard pontoon length [m]	45.0	1.00
Bow pontoon length [m]	41.0	0.91
Draft [m]	16.00	0.36

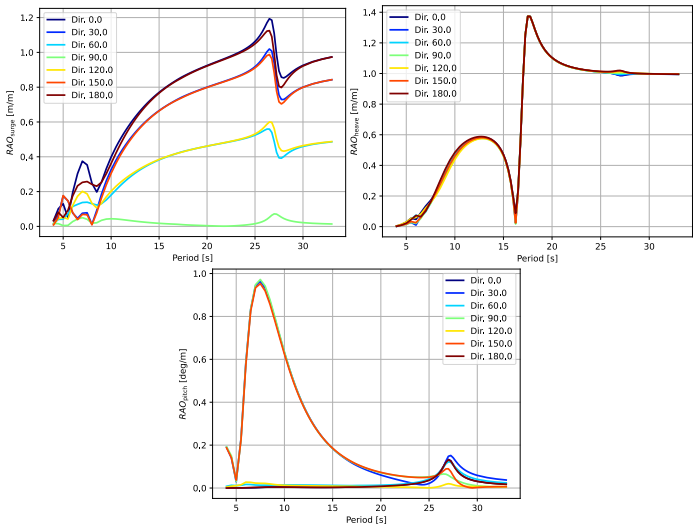

Figure 2. RAOs for Surge, Heave and pitch motions across six different headings.

Due to the insufficient water depth of the wave basin to accommodate

the original 2000 m mooring system, the mooring lines were truncated to fit within the basin's constraints while preserving the static characteristics of the full-scale design, see (Simos et. al., 2023). The truncated mooring system (model-scale) consists of four lines: two of them attached to the designated bow column of the platform, and one to each of the starboard and port columns. The lines feature an anchor-to-depth radius of 1.37. Each line consists of a load cell (attached to the fairlead to measure the line tension), a chain segment, a wire segment, a spring, and another chain segment anchored to the wave basin floor. The use of springs in the equivalent scale-mooring system allows the mooring lines to be shortened while still simulating the restoring forces and elastic behavior of the full-scale system, enabling the emulation of the plane stiffness of the mooring system even with equivalent shorter lines. An schematic representation of the mooring system is provided in Figure 3 and its main details are summarized in Table 3.

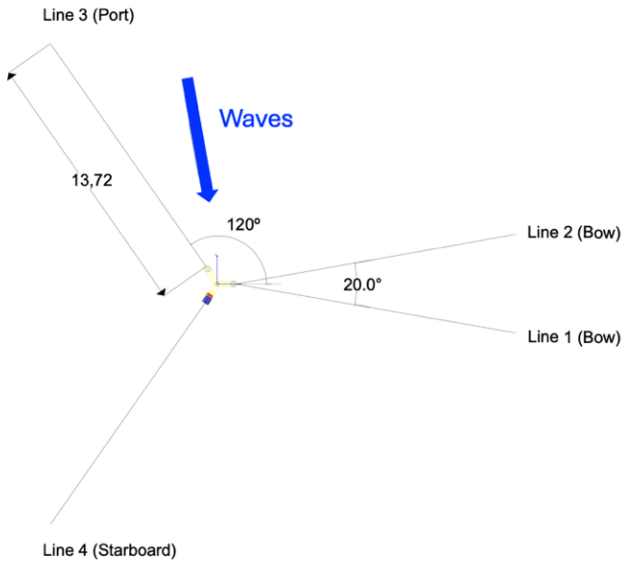

Figure 3. Experimental mooring configuration.

Table 3. Main properties of the mooring system

	Full Scale	Model Scale (1:45)
Anchor Depth	495m	11m
Anchor Radius from center	677,25	15,05m
Fairlead depth	16m	0,36m
Bottom segment material	Steel Chain	Steel Chain
Length	33,75m	0,750m
Linear Mass Density	139,73kg/m	0,069kg/m
Spring	--	--
Length	57,83m	1,285m
Linear Mass Density	1093,5kg/m	0,540kgg/m
Intermediate segment material	Wire	Wire
Length	525,09	11,691m
Linear Mass Density	20,25kg/m	0,010kg/m
Top segment material	Steel Chain	Steel Chain
Length	22,50m	0,500m
Linear Mass Density	139,73kg/m	0,069kg/m

Experimental Matrix

The test matrix comprises a subset of three DLCs selected from over 30 DLCs included in the experimental campaign, which were chosen based on the guidelines provided in (DNV GL AS, 2016). These DLCs were tested for two distinct headings relative to the wave direction. The selected subset corresponds to waves incident at an angle of 95deg relative to the pontoon designated as the platform's bow (see Figure 3).

The characteristics of the selected DLCs are provided in Table 4. These include two environmental conditions characterized by significant wave height (Hs) and peak period (Tp) associated with two different wind speeds: one below rated wind speed (Test#1) and one above it (Test#2), thus different control regions are tested.

The below rated wind speed (10.59m/s) turbine's control strategy assumes the blade pitch angle constant and close to zero with turbine velocity controlled to optimize energy by the torque control. Above rated wind speed the controller assumes saturated toque at the rated value and controls the blade pitch angle to maintain the rated turbine speed. According the ROSCO open controller strategy that the SiL was based, at the rated wind speed a peak shaving was applied to smooth the thrust peak of the rotor reaction at the tower. This strategy is designed to reduce the load at the tower, platform and mooring lines.

Table 4. Details of the selected DLCs

Test	Type	H_S [s]	T_P [s]	$Wind_{speed}$ [m/s]	Type
1	JONSWAP	2.01	8.54	8.59	NTM
2	JONSWAP	2.16	12.66	12.59	NTM
3	JONSWAP	10.93	16.00	19.50	NTM

Additionally, the selected subset includes an extreme wave condition with 50y return period. The mean wind velocity of this DLC was chosen to ensure that it operates continuously throughout the test, as required in (DNV GL AS, 2016).

All the turbulent wind time series in the experiential matrix were generated using TurbSim (Jonkman and Kilcher, 2012), a tool that provides a high-fidelity numerical representation of a full-field turbulent wind flow. The wind time series generated followed the Normal Turbulence Model (NTM) with a turbulence intensity corresponding to Class B (see (Carmo et. al., 2024) for a detailed assessment of the turbulent wind records generated using TurbSim). The TurbSim-generated output file was used as an input for both the experimental tests and numerical simulations, ensuring consistency of the wind conditions. For the sake of illustration, the spectra of the wind turbulence series for the three tests are presented in Figure 4.

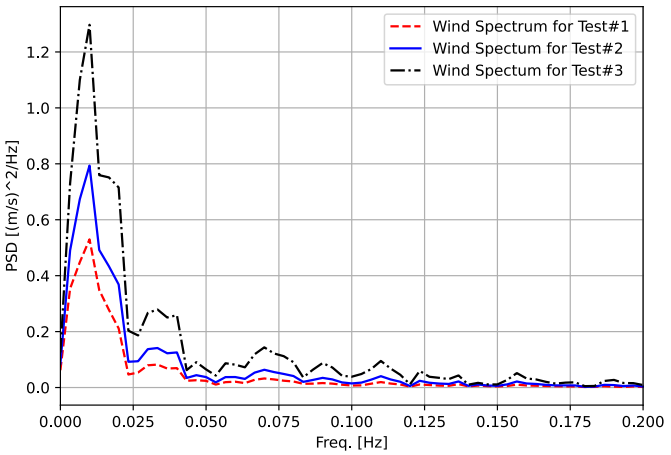

Figure 4. Wind spectra for the turbulent time series for Tests#1, #2 and #3.

NUMERICAL MODELLING

The numerical simulations were conducted using OpenFAST v3.5.2, an open-software that enables time-domain simulation of the coupled dynamics of FOWTs under aerodynamic and hydrodynamic loadings. OpenFAST computes wave forces using a combination of radiation/diffraction loads, modeled through Cummins's approach, see (Cummins, 1962), in the HydroDyn module, with frequency-dependent coefficients pre-calculated in the frequency domain using WAMIT v7.0.6, and quadratic drag forces derived from Morison's equation (Morison et. al., 1950). The mooring system dynamics were simulated using the coupled MoorDyn v2.0.0 module, which employs a lumped-mass model to represent the behavior of mooring lines.

The OpenFAST model setup was configured based on the measured characteristics of the experimental model (refer to Table 2 and Table 3) extrapolated to full scale, ensuring the representativeness of the simulations. In this context, the AeroDyn module, which calculates aerodynamic loads using the dynamic Blade-Element/Momentum (DBEM) approach combined with an unsteady airfoil aerodynamic (UA) model, was configured to exclude tower loads and shadow effects, aligning with the current SiL implementation, see (Carmo et. al., 2024).

The structural dynamics were computed using the ElastoDyn module. In this setup, the degrees of freedom associated with the tower modes (fore-aft and side-side) and the blade modes (flapwise and edgewise) were disabled, as these dynamics are not represented by the experimental scale model.

Numerical Simulations

As outlined in the Introduction, the first step of this work aimed at validating the numerical simulations using the experimental data. This validation was performed by comparing the outputs of the time-domain simulations with the experimental measurements through statistical analysis for the DLCs listed in Table 4. To ensure accurate comparisons, the wave elevation time series recorded during the wave calibration phase - conducted prior to placing the model in the wave basin - were used as input for the numerical simulations, along with the wind turbulent series generated using TurbSim (see subsection Experimental Matrix).

The validated numerical model was subsequently utilized to generate 10 realizations of each DLC listed in Table 4, employing different random seeds under turbulent wind conditions. Additionally, the same OpenFAST model was applied to simulate 10 realizations of the same DLCs, assuming steady wind conditions defined by an exponential profile with a shear exponent of 0.14. In total, 60 cases were simulated (30 with turbulent wind and 30 with steady wind), providing the data used to evaluate the impact of turbulence on mooring line loads, as discussed in the following section.

Each simulation spanned 4 hours in full scale, with the initial 2000s excluded to eliminate transient platform responses, leaving approximately 3.5h of time series for analysis. This ensures that the time series are sufficiently long to capture the statistical variability of mooring line tensions.

The simulations were carried out in batch mode using a MATLAB script developed in-house, allowing multiple simulations to run simultaneously. Each simulation was assigned to a core of a standard six-core computer, with an average runtime of 1.5h. This setup allowed all simulations to be completed in approximately 16h.

RESULTS

The experimental tests considered in this study for the validation phase of the numerical model focused only on wind turbine operational conditions. The experimental time series span approximately 2.5 hours. However, the initial 2000s were excluded to eliminate the transient responses of the platform model, this adjustment reduced the usable duration of the time series for analysis to 8000s. The agreement between the numerical model results and the experimental data is evaluated and discussed in the following subsection.

Validation of the Numerical Model Set Up

First, the dynamic responses of the platform as tested in the wave basin are assessed by means of decay data of the six degrees of freedom and their comparison with the numerical estimations. For the sake of illustration, Figure 5 presents the surge motion records from the decay test with an initial amplitude of 20m, showing experimental data without the umbilical (dashed red line) and numerical results (blue line). The comparison shows good agreement between the experimental and numerical data.

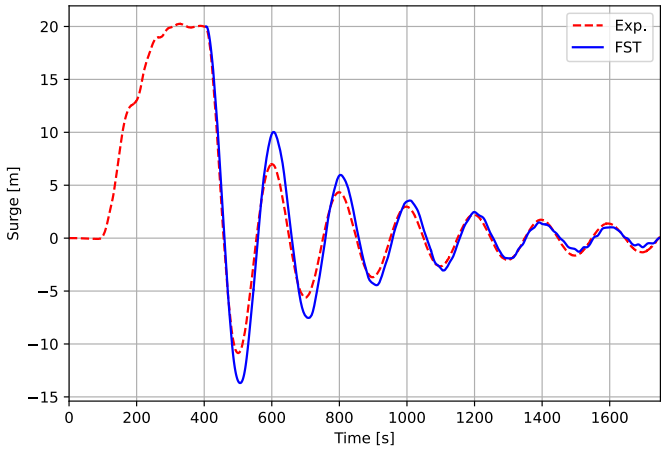

Figure 5. Experimental and numerical decay test records.

For conciseness, the comparison of the other motions is presented in Table 5 through the measured and estimated natural periods. This table includes the target values for each motion natural period, the experimental measurements for the mooring model-scale platform without the umbilical ($T_{Exp.\ w/o\ umb.}$), and with the umbilical ($T_{Exp.\ w/umb}$). During the experimental campaign, the umbilical cable was used to supply power to the set of fans and to accommodate a cluster of sensor cables (i.e. load cells and wave probes). It was suspended from the laboratory ceiling by a set of two springs and connected to the platform in the same direction as the designated bow of the hull, as illustrated in Figure 6. It is important to note that the spring-umbilical cable arrangement cannot be modeled in the numerical simulation tools due to the adopted air-hanged configuration. Further improvements to the configuration of the umbilical power cable required for the hybrid model-scale tests have been left as a future work.

The numerical results show a reasonable agreement between the target values and the experimental data without the umbilical cable. However, the natural periods measured with the umbilical cable connected exhibit significant discrepancies from the target values, particularly for the surge and sway motions of the platform, with differences of up to 13%.

Table 5. Comparison of estimated and measured surge and sway natural periods.

Motion	T_{Target} [s]	T_{FST} [s]	$T_{Exp.\ w/o\ umb.}$ [s]	$T_{Exp.\ w/umb.}$ [s]
Surge	198.5	198.7	199.2	173.5
Sway	194.3	193.8	190.4	188.6
Heave	17.1	17	17.2	17.7
Roll	27.3	27.2	27.7	27.4
Pitch	27.2	27.1	27.3	27.5
Yaw	55.9	54.6	53.8	53.5

Regarding the tensions of the mooring lines, Figure 7 illustrates the numerical and experimental time series for Test #1. The data is provided for each mooring line (see Figure 3 for the line nomenclature) with experimental records shown in red and numerical results in blue. The comparison indicates that the numerical data generally fairly agrees with the experimental measurements.

However, a better fit is observed for the port and starboard lines compared to the bow lines. As previously noted in the analysis of the natural periods, this discrepancy between the numerical and experimental data for the bow lines is likely to be related to the effects of the umbilical cable, connected to the platform in the same direction as the bow lines (see Figure 6). The umbilical configuration used during the experimental campaign may have induced larger surge motions in the platform that were not captured by the numerical model. This is because the model relies in hydrodynamic forces (see Figure 2) to compute platform responses and does not explicitly account for the umbilical and its dynamics effects. As a result, deviations are observed in the amplitude and frequency of the surge motion, as well as in the dynamic behavior of the bow mooring lines.

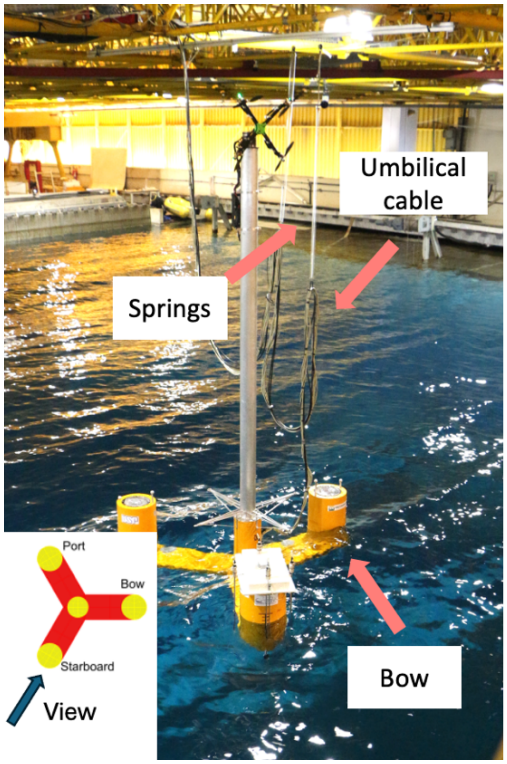

Figure 6. Set-up configuration of the scale model showing the umbilical layout.

The selection of Test #1 for illustrating the time series is arbitrary, but it stands as a representative example of the observed behavior between the numerical and experimental mooring line tension time records across the three tests. A quantitative assessment of the agreement between the numerical and experimental results is presented in Table 6. This table provides key statistical parameters, including the maximum values and the variance (σ^2) of the time series, and the R^2 score. The R^2 score has been included as a measure of the agreement between the numerical and experimental time series. The use of this score is possible because both wave and wind time series, as previously noted, were identical for the numerical and experimental simulations.

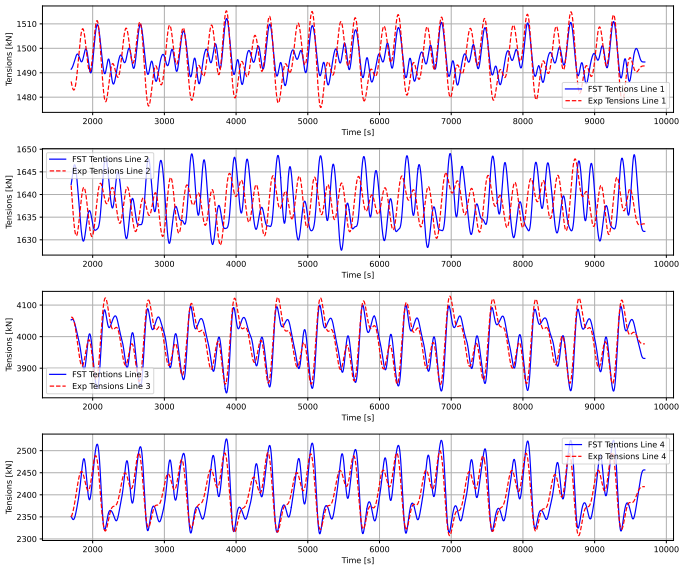

Figure 7. Mooring line time numerical and experimental time series for Test#1.

The results for Test#1, which correspond to an under-rated mean wind speed, demonstrate good agreement between the maximum tension values from the numerical and experimental time series for all four lines, with differences of less than 1%. In terms of variance, Lines 3 and 4 show good agreement between numerical and experimental results, while Lines 1 and 2 show poorer agreement. This discrepancy is hypothesized to be attributed to the influence of the umbilical during the model scale experimental campaign. A similar trend is observed in the R^2 scores, which indicate better agreement between numerical and experimental data for Lines 3 and 4 compared to Lines 1 and 2.

For the DLC with wind speeds above the rated wind, a similar tendency can be observed. The maximum tension values show good agreement for all four lines, with differences remaining below 1%. Regarding the variance and R^2 scores, both parameters show a trend consistent with Test#1, with better alignment between the numerical and experimental data for Lines 3 and 4. However, for this DLC, the variance and R^2 scores suggest a generally poorer agreement compared to Test#1.

Test #3, which represents a wave condition with a 50-year return period, also shows good agreement between the maximum values of the numerical and experimental time series, with differences smaller than 1%. Similar to Test #1 and Test #2, the variance and R^2 score show better agreement for the port and starboard lines. In this case, one may observe that the maximum values for all four lines are smaller than those observed in Tests #1 and #2. This outcome is attributed to the wind velocity being close to the cut-out wind speed, where the wind turbine produces less thrust compared to wind speeds closer to the rated wind speed. Similarly, the variance is smaller when compared with Tests #1

and #2.

These results confirm that the numerical model shows good agreement with the experimental data for both DLCs featuring under-rated and over-rated wind speeds, as well as with the increase of wave height. Nonetheless, some discrepancies are observed, likely related to the influence of the umbilical in the model scale. A detailed evaluation of the impact of the umbilical cable in the experimental results is left for future work.

Table 6. Statistical parameters of the numerical and experimental mooring line dynamics

	Lines	Type	Max. [kN]	σ^2 [kN^2]	R^2
Test#1	L#1	Experimental	1515.31	99.21	0.49
		Numerical	1512.12	36.49	
	L#2	Experimental	1647.89	13.90	-0.57
		Numerical	1649.19	28.92	
	L#3	Experimental	4133.29	5733.75	0.82
		Numerical	4101.26	5196.49	
	L#4	Experimental	2510.33	3054.95	0.71
		Numerical	2525.60	3311.93	
Test#2	L#1	Experimental	1530.71	152.62	0.49
		Numerical	1521.04	134.65	
	L#2	Experimental	1648.71	26.49	-0.29
		Numerical	1643.96	13.54	
	L#3	Experimental	4099.42	5486.15	0.65
		Numerical	4106.40	6367.22	
	L#4	Experimental	2544.85	2120.85	0.63
		Numerical	2527.04	2810.66	
Test#3	L#1	Experimental	1531.59	49.15	0.32
		Numerical	1539.69	44.06	
	L#2	Experimental	1630.60	14.68	-0.30
		Numerical	1640.74	42.52	
	L#3	Experimental	3829.82	2101.63	0.60
		Numerical	3794.26	633.98	
	L#4	Experimental	2697.59	1022.79	0.58
		Numerical	2683.49	368.14	

Wind Turbulence and Mooring Line Tensions

The results of the time-domain simulations in OpenFAST, conducted to evaluate the effects of wind turbulence on mooring line tensions, are summarized in Table 7. This table presents the maximum and minimum values from the 10 realizations of each test (see Table 4) for each mooring line, for both the wind turbulent conditions (TRB) and steady wind conditions (STD). These statistics have been complemented by the Most Probable Maximum (MPM), estimated following DNV's guidelines, see (DNV AS, 2021), which define this parameter as:

$$MPM = \mu - 0.45 \cdot \sigma \quad (1)$$

where μ and σ stand for the mean and variance of the peaks (i.e. the maximums values observed in each of the 10 realizations of each DLCs).

The comparison of the MPM results indicates that the differences between turbulent and steady wind conditions are limited to 4.5% for Test#1 and 2.9% for Test#2. The maximum difference for Test#1 is observed in the starboard line, while for Test#2, it is observed in the port line. These differences correspond to 108kN and 70kN, respectively. For Test#3, where wave excitation (corresponding to a 50y return period sea state with a H_s of 10.93m and T_p equal to 16s) is expected to dominate platform motions, the maximum difference in MPM is observed in Line 2, with a difference of 2.5%, equivalent to 58kN.

A similar trend is observed when comparing the maximum values recorded during the 10 realizations of each DLC. Lines 3 and 4 exhibit the largest differences for tests with wind speeds near the rated wind velocity, with 4.6% (Line 4 in Test#1) and 3.1% (Line 4 in Test#2). These differences correspond to 111kN and 117kN, respectively. For Test#3, the largest differences are again observed in the bow lines, with Line 2 showing a difference slightly below 5%, or 127kN.

Table 7. Mooring value statistics for turbulent and steady wind conditions obtained from numerical simulations.

		L#1	L#2	L#3	L#4
Test#1					
TRB	MPM [kN]	1536.84	1640.58	4162.51	2526.25
	Max. [kN]	1546.62	1646.21	4167.38	2533.17
	Min. [kN]	1535.02	1638.26	4159.20	2522.57
STD	MPM [kN]	1524.31	1634.29	4076.51	2417.92
	Max. [kN]	1530.48	1640.11	4082.21	2422.13
	Min. [kN]	1522.72	1633.22	4072.28	2417.73
Test#2					
TRB	MPM [kN]	1570.04	1667.31	4231.47	2487.23
	Max. [kN]	1578.29	1690.61	4246.75	2500.30
	Min. [kN]	1566.26	1665.63	4228.45	2480.33
STD	MPM [kN]	1552.36	1666.44	4107.11	2417.07
	Max. [kN]	1563.38	1681.01	4129.00	2425.10
	Min. [kN]	1548.49	1655.64	4097.31	2413.83
Test#3					
TRB	MPM [kN]	2263.15	2400.39	4841.96	3346.44
	Max. [kN]	2518.08	2745.20	5354.48	3611.63
	Min. [kN]	2140.62	2251.31	4564.18	3243.41
STD	MPM [kN]	2257.88	2342.07	4830.42	3341.13
	Max. [kN]	2425.37	2617.43	5275.81	3522.09
	Min. [kN]	2220.39	2334.82	4730.47	3324.72

For the minimum values, the largest differences are found in Test#1 (Line 4) and Test#3 (Line 1), with values of 4.3% and 3.6%, corresponding to 104kN and 83kN, respectively.

Notably, Test#3 induced the largest maximum values and the largest differences between the minimum and maximum mooring line tensions, despite corresponding to the DLCs with the smallest mean turbulent thrust provided by the wind turbine.

Regarding the wind turbine thrust, the mean values for the turbulent cases in Tests#1 and #2 are 2136.2kN and 2166.18kN, respectively, while for the steady wind cases, the values are 2149kN for Test#1 and 2217.21kN for Test#2. For Test#3, the mean thrust values are 1348.31kN for the turbulent case and 1173.13kN for the steady case. The differences lead to larger offsets for Test#1 and #2, with mean values of 55.89m and 56.58m, respectively, for the turbulent cases, and 56.67m and 57.49m for the steady cases. In contrast, for Test#3, the mean offset value was 38.48m for the turbulent case and 34.32m for the steady case. It is important to note that the mean values for the turbulent cases, both in thrust and offset, may be slightly smaller than those recorded for the steady wind conditions for the same tests due to the larger variance of the time signals.

Therefore, the results show that the tests with wind speeds closer to the rated wind exhibit a larger offset than Test#3, as expected. More specifically, the results suggest that line tensions in Tests#1 and #2 are likely more influenced by the platform's mean offset and, perhaps, the turbulent wind spectrum. By contrast, for extreme sea states, the mooring dynamics appear to be dominated by wave excitation. In this context, Figure 8~Figure 10 presents the mooring line tension spectra for all the

tests performed and the all the mooring lines, adding a more detailed assessment of the dynamic responses of the mooring lines. Each subplot of these figures contains six lines, representing the mean spectra of the ten realizations for each turbulent case (black line), the mean spectra of the ten realizations for the steady case (blue line), and the 5th and 95th percentile values for both the ten realizations of the turbulent (green dashed lines) and steady case (red dashed lines) for each test and mooring line.

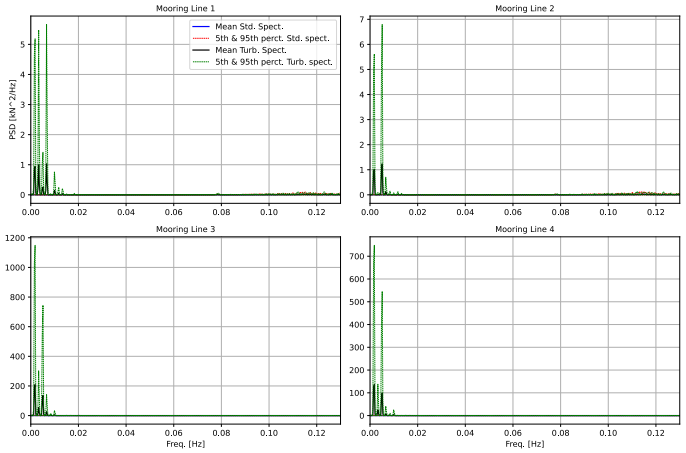

Figure 8. Mooring line tensions spectra for test#1

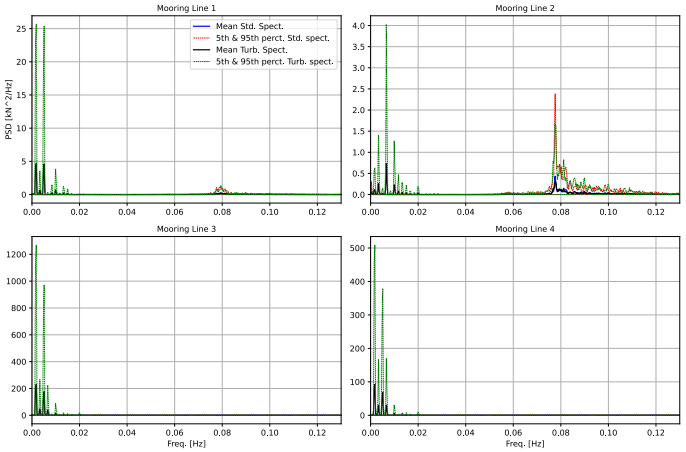

Figure 9. Mooring line tensions spectra for test#2

The spectra for Tests #1 and #2 (see Figure 8~Figure 9) indicate that the dynamics in all mooring lines show a response in the low-frequency range for the turbulent wind conditions (see Figure 4), while for the realizations of the same tests with steady wind, this response is not observed. Therefore, the mooring lines' dynamic response for the Tests #1 and #2 for the turbulent wind conditions in the low-frequency range is likely associated with the wind spectra. Nonetheless, it is important to note that the dynamic effects imposed by the turbulent wind, even for these cases with mean wind speeds close to the rated wind, are limited, as shown previously in the statistical results presented in Table 7. For Test#2, in Line 2 (i.e., the second plot in the second row of the figure), it is also possible to observe the responses induced by wave excitation.

Figure 11 shows the mooring line tension spectra for Tests #1 and #2, disregarding the frequency range where the wind spectra present its energy. This figure is provided for the sake of illustration of the tension spectra induced by wave excitation, where small differences can be seen between the mean spectra (turbulent and steady cases) as well as the 95th percentiles for both turbulent and steady cases, particularly for Lines 3 and #4.

Regarding Test#3 (see Figure 10), the mooring line dynamics are dominated by sea excitation, with spectra for both turbulent and steady cases showing good agreement. This confirms the trend identified in the statistical data from the simulations (see Table 7), where the results show that wind turbulence has a limited effect on the mooring line dynamics for Test#3.

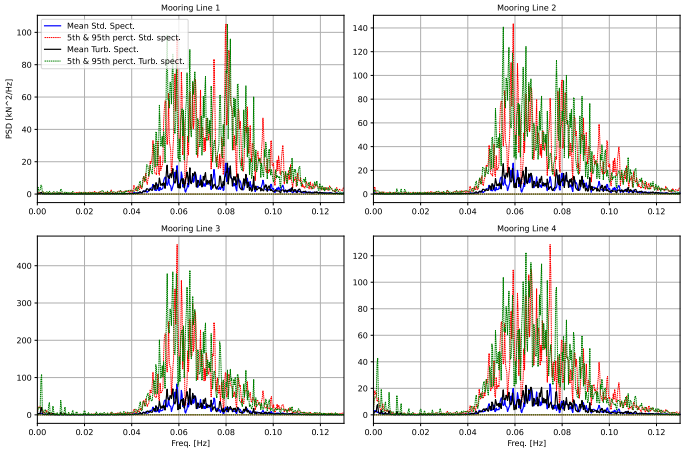

Figure 10. Mooring line tensions spectra for test#3

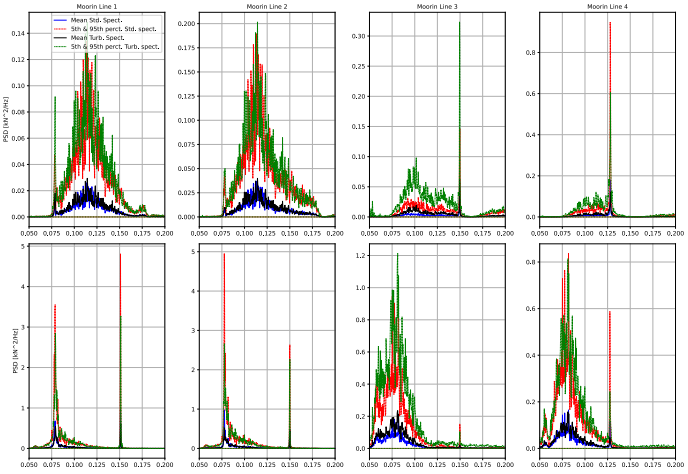

Figure 11. Mooring line tensions spectra for each line (subplots in columns) and tests #1 and #2 (subplots in rows)

The responses observed near 8 seconds, more evident for Lines 1 and 2 in Tests #2 and #3 (Figure 11), seem to be related to the platform's pitch dynamic response. This is supported by the pitch RAO, which shows a local maximum close to 8 seconds, and by the analysis of the pitch motions, which also confirms a response in this frequency range. Furthermore, it is also important to note that the tower and blade structural dynamics responses were disabled, as described in the previous section titled "Numerical Simulations". A dedicated investigation into this response in the high-frequency range has been left for future work.

CONCLUSIONS

In this paper, an assessment of the effects of wind turbulence on the

mooring line tensions was conducted using a semisubmersible FOWT as a reference to withstand the IEA-15MW wind turbine described in (Simos et. al., 2023). Time series from experimental data with a 1:45 model scale were adopted to validate the setup of the OpenFAST numerical model for selected environmental conditions. The tested environmental conditions include one wind speed above the rated wind and another wind speed below the rated wind, allowing the assessment of two different control regions of the wind turbine. Additionally, an extreme environmental condition was assessed. The comparison of the time series and the statistical parameters shows fair agreement between the numerical and experimental results, thus supporting the reliability of the numerical setup. The same numerical setup was used to simulate 10 realizations of each of the selected environmental conditions with turbulent and steady winds.

The assessment of the results indicates that for the MPM, the differences between the turbulent and steady wind conditions are limited. This suggests that, for an early assessment of a FOWT project, steady wind conditions could be adopted as a reliable characterization of the mooring line dynamics. A similar behavior was observed for the maximum and minimums of the numerical realizations carried out for each test. Therefore, it is possible to conclude that the turbulence effects on the design tensions are limited.

Notwithstanding this, the results also showed that for environmental conditions with wind speeds close to the rated wind of the wind turbine (i.e., 10.59m/s), the mooring line dynamics are likely dominated by wind forces. On the other hand, environmental conditions associated with extreme wave conditions (usually correlated with higher wind speeds, which result in lower wind turbine thrust) appear to be dominated by the wave spectra. These effects on the dynamics of mooring line tensions indicate that considering wind turbulence is likely a critical factor for properly calculating the cumulative fatigue damage of the mooring lines.

Future work envisaged for the research topic addressed in this work includes a comprehensive numerical assessment to evaluate the effects of turbulence across different wind speeds within the wind turbine's control regions. Additionally, it will investigate the influence of various wind turbulence models on the MPM and fatigue life, as well as assess the impact of second-order motions. Future studies will include assessing the impact of the scale on experimental measurements, analyzing the response dynamics of the platform and mooring tensions, and examining alternative umbilical configurations. Moreover, a dedicated analysis is planned to assess the accuracy of the numerical model based on the Morison coefficients adopted for the columns and pontoons in this study.

ACKNOWLEDGEMENTS

This work was developed as part of the R&D project conducted by Petrobras and the University of São Paulo entitled “Disruptive Technologies for Floating Offshore Wind in Deep Water” (agreement Petrobras #0050.0129630.24.9). Authors wish to thank Petrobras for the funding of this project and the Brazilian National Petroleum Agency (Agência Nacional do Petróleo, ANP) for providing the regulatory framework under which this funding takes place. Alexandre Simos also acknowledges the Brazilian National Research Council (CNPq) for his research scholarship (grant # 311928/2023-4).

REFERENCES

C. de Mello, P., Mas-Soler, J., M. Monaro, R., Simos, A. N. and Silva, D.F.C (2025). "Experimental emulation of shutdown and start-up procedures in wave basin tests of a 15mw floating offshore wind turbine" *(submitted for publication)*.

Carmo, L. et al., 2024. "Numerical modeling of wave basin experiments of a floating wind turbine with active thrust emulation: A discussion of important aspects". *Ocean Engineering*, 309, p. 118379.

Cummins, W. (1962). *The impulse response function and ship motion*. Department of the Navy, David W. Taylor Model Basin, Hydromechanics Laboratory.

DNV AS (2021). *DNV-OS-E301: Position Mooring*. DNV.

DNV GL AS (2016). *Loads and site conditions for wind turbines*. DNV GL.

EQUINOR (2023). "Hywind Tampen". [Online] *Available at: https://www.equinor.com/energy/hywind-tampen* [Accessed 12 1 2025].

EQUINOR, (2022). "Hywind Scotland". [Online] *Available at: https://www.equinor.com/energy/hywind-scotland* [Accessed 12 01 2025].

Gaertner, E., Rinker, J., Sethuraman, L., Zahle, F., Anderson, B., Barter, G., Abbas, N., Meng, F., Bortolotti, P., Skrzypinski, W., and Scott, G (2020). *Definition of the IEA 15-megawatt offshore reference wind turbine*. IEA.

Hall, M. (2024). "Generalized Quasi-Static Mooring System Modeling with Analytic Jacobians". *Energies*, 12(13), p. 3155.

Hall, M., Housner, S., Ogden, D.; Zalkind, D., Barter, G. and Bortolotti, P. (2022). *RAFT (Response Amplitudes of Floating Turbines)*.

IEA Wind TCP (2022). "IEA Wind TCP Task 56". [Online] *Available at: https://iea-wind.org/task-56-oc7-project-offshore-code-comparison-collaboration-7/* [Accessed 12 1 2025].

Jonkman, B. J. and Kilcher., A. L. (2012). *TurbSim user’s guide* National Renewable Energy Laboratory, Golden, CO, USA.

Karimi, M., Hall, M., Buckham, B. & and Crawford, C. (2017). "A multi-objective design optimization approach for floating offshore wind turbine support structures". *Journal of Ocean Engineering and Marine Energy*, 3, pp. 69-87.

Lauria, A., Loprieno, P., Rizzo, F., Severini, A., Foti, D., Leone, E., Francone, A, A., and Tomasicchio, G.R. (2024). "On the effects of wind and operating conditions on mooring line tensions for floating offshore wind turbine". *Applied Ocean Research*, 152, p. 104197.

Mas-Soler, J., do Amaral, G.A., da Silva, L.Z., Malta, E.B., Carmo, L.H.S., Ruggeri, F., and Simos, A.N. (2022). "A parametric optimization approach for the initial design of FOWT’s substructure and moorings in Brazilian deep-water fields". *Journal of Physics: Conference Series*, 2362(1), p. 012025.

Morison, J., Johnson, J. and Schaaf, S. (1950). "The force exerted by surface waves on piles". *Journal of Petroleum Technology*, 2(5), pp. 149-154.

Piscopo, V. and Scamardella, A. (2023). "Incidence of wind spectrum and turbulence intensity on the design of mooring systems for floating offshore wind turbines". *Ocean Engineering*, 290, p. 116377.

Provence Grand Large (2024). "Provence Gand Large". [Online] *Available at: https://www.equinor.com/energy/hywind-tampen* [Accessed 12 1 2025].

Simos, A.N., Salles, M.B., Monaro, R.M., Martins, M.R., Mas-Soler, J., Gay, A., Franzini, G.R., Carmo, B.S., Pesce, C.P., Morishita, H.M., and Carvalho e Silva, D.F. (2023). "Deep-Water Floating Offshore Wind Turbine Concept for Subsea Water Injection". *In Offshore Technology Conference Brasil (OTC)*.

Technomar (2024) ."Engineering Projects". [Online] *Available at: https://www.technomar.com.br/produto-e-servico/projetos-de-engenharia/ [Accessed 17 1 2025]*.